JOURNAL OF SOLID STATE CHEMISTRY **132,** 257–266 (1997)
ARTICLE NO. SC977438

HREM Image Analysis up to Structure Determination of $SbCrSe_3$: A New 1D Ferromagnet

V. V. Volkov,*,† G. Van Tendeloo,* J. Van Landuyt,* S. Amelinckx,* E. E. Busheva,† G. G. Shabunina,† T. G. Aminov,† and V. M. Novotortsev†

*EMAT, University of Antwerp (RUCA), Groenenborgerlaan-171, B-2020, Antwerpen, Belgium; and
†N.S. Kurnakov Institute of General & Inorganic Chemistry, RAS, Leninsky Prosp.-31, 117907 Moscow, Russia

Received January 30, 1997; accepted April 22, 1997

The combined use of high-resolution electron microscopy (HREM), image analysis, and X-ray refinement techniques enabled us to determine the structure of $SbCrSe_3$ as orthorhombic (space group *Pnma*, $a = 9.1689(30)$, $b = 3.7957(12)$, 13.4637(44) Å). The structure model of $SbCrSe_3$ has been derived directly from the HREM image along the [010] direction. It consists of edge sharing $CrSe_6$ octahedra forming double rutile chains along the *b*-axis and separated by Sb atom columns located approximately in pentagonal tunnels of Se atoms. The structural model was refined by the full profile XRD powder Rietveld method. The compound $SbCrS_3$ ($a = 8.68$, $b = 3.62$, $c = 12.88$ Å) is isostructural to $SbCrSe_3$. Below the Curie temperature both compounds exhibit features which suggest 1D ferromagnetism.

1. INTRODUCTION

The compounds $MCrX_3$, belonging to a subgroup of the MTX_3 group of ternary chalcogenides (M a nontransition metal, T a transition metal, and X = S, Se), occur in a number of structure types. They are likely to have interesting magnetic properties related to 1D–3D magnetism since Cr is a transition 3*d* element. These properties are determined by the structural type of the compound and by the M cations. If $M = Ln$, a rare earth 4*f* element, the magnetic properties can even be more complex than for a nontransition element. MTX_3 compounds with $T = Cr$ are less studied than other transition metal chalcogenides. In particular, there are reports on sulphides,

$InCrS_3$	((1), cubic cell, S.G. $Fd3m$, spinel of Al_2MgO_4 type),
$ScCrS_3$	((2), rhombohedral, S.G. $R\bar{3}m$, of $NaCrS_2$ type),
$UCrS_3$	((3), orthorhombic, S.G. *Pnma*, of $UCrS_3$ type),
$LaCrS_3$	((4), monoclinic, S.G. $P2/m$, of $LaCrS_3$ type);

and selenides,

$PCrSe_3$	((5), monoclinic, S.G. $C2/m$, of $PFeSe_3$ type),
$ThCrSe_3$	((6), orthorhombic, S.G. $Pna2_1$, of $UCrS_3$ type),
$GaCrSe_3$	((7)), orthorhombic, S.G. *Pnma*, possibly of Sn_2S_3 type),
$LnCrSe_3$	(Ln = Ce(8), La(9), orthorhombic, S.G. *Pnma*, of $CeCrSe_3$ type).

Studies have been reported on misfit layer compounds $(LnS)_nCrS_2$, $n = 1.20$–1.23 (Ln = La (10), Ce, Pr, Nd (11)), containing CrS_2 sandwiches as well. In most cases the structures are formed by CrX_6 polyhedra (either octahedra or trigonal antiprisms) stacked in different ways, which may lead in principle to the formation of either 1D, 2D, or 3D infinite networks of CrX_6 octahedra responsible for the dimensionality and the type of the magnetic interactions. These data indicate that the symmetry and the type of $MCrX_3$ structure formed should be very sensitive to the M cation.

On the other hand there is a large class of semiconducting magnetic crystals of the type MCr_2X_4 (M = metal, X = S, Se, Te). Many of these crystallize in the spinel-type structure and display very interesting 3D-magnetic properties, including ferromagnetism. The microscopic theory of which is not well developed yet because of the complexity of the problem. It was shown recently that nonmagnetic Sb can partially replace Cr resulting in the formation of a new spinel compound $Cu[Cr_{1.5}Sb_{0.5}]S_4$ which exhibits a spin glass magnetic behavior (12). This type of substitution can generally be used to block a number of exchange channels in the structure and therefore to reduce the dimension of the magnetic interactions. If the amount of Sb exceeds the critical concentration for isomorphous substitution in the spinel type, a new structure type can be formed.

The present work will demonstrate the use of high-resolution electron microscopy (HREM) in combination with

0022-4596/97 $25.00

X-ray powder methods for the structure determination of new compounds with an unknown structure. The compounds $SbCrX_3$ (X = S, Se) belong to the class of ternary chalcogenides mentioned above. They were recently discovered in the sections Sb_2X_3–Cr_2X_3 of the more complex phase diagrams of chromium chalcogenides with antimony and some transition metals as a result of a systematic search of new magnetic semiconductors (13). Attempts to determine their structure by the traditional X-ray methods, however, were unsuccessful.

We shall show that $SbCrX_3$ (X = S, Se) form a structure of a new type, intermediate between those of $GaCrSe_3$ (7) and $CeCrSe_3$ (8); moreover, they are expected to possess 1D ferromagnetic properties.

2. EXPERIMENTAL PROCEDURE

Powdered samples of $SbCrX_3$ (X = S, Se) were prepared from high grade purity elements: Sb, 99.9%; S or Se, 99.6%; and Cr, 99.5% (Koch-Light). Mixtures of the elements of nominal composition were encapsulated in evacuated fused quartz tubes and subjected to a two-step sintering procedure. A first annealing treatment at 750°C for 4 days was followed by an additional one at 600°C for 5 days. After such heat treatments the substances were carefully ground and annealed again at 750°C for 7 days and subsequently at 500°C for 14 days. The phase composition of the samples was checked by differential thermal analysis and X-ray phase analysis. After the second annealing only one thermal effect was detected by DTA, i.e., incongruent melting of $SbCrSe_3$ at 790°C. The $SbCrSe_3$ samples were subjected to a third annealing treatment at 750°C for 12 days to check the stability and the reproducibility of the peak positions in the final XRD pattern.

The high-resolution electron microscopy (HREM) and the electron diffraction (ED) studies were carried out using a JEOL 4000EX microscope operating at 400 kV. The reciprocal space studies were done in a Philips CM-20 electron microscope. Sample preparation for ED studies was very straightforward: the powdered substances were carefully crushed and the fragments were glued onto copper grids. For HREM observations we mostly used specimens prepared by ion beam milling of a sample of $SbCrSe_3$ powder mixed with epoxy glue. Such specimens allowed us to avoid the preferential orientation due to a strong natural anisotropy of the prismatic microneedles of substances and to obtain HREM images along the *b*-axis.

To characterize the morphology, the elemental composition, and the lattice parameters of the phases of interest, scanning electron microscopy (SEM), energy dispersive X-ray (EDX), and X-ray powder diffraction analysis (XRD) were performed. For this purpose a JEOL GSM-T220A scanning electron microscope, equipped with an EDX KEVEX system for microprobe elemental analysis, and a Philips PW3710 X-ray powder diffractometer were used. The magnetic susceptibility was measured with the Faraday balance method.

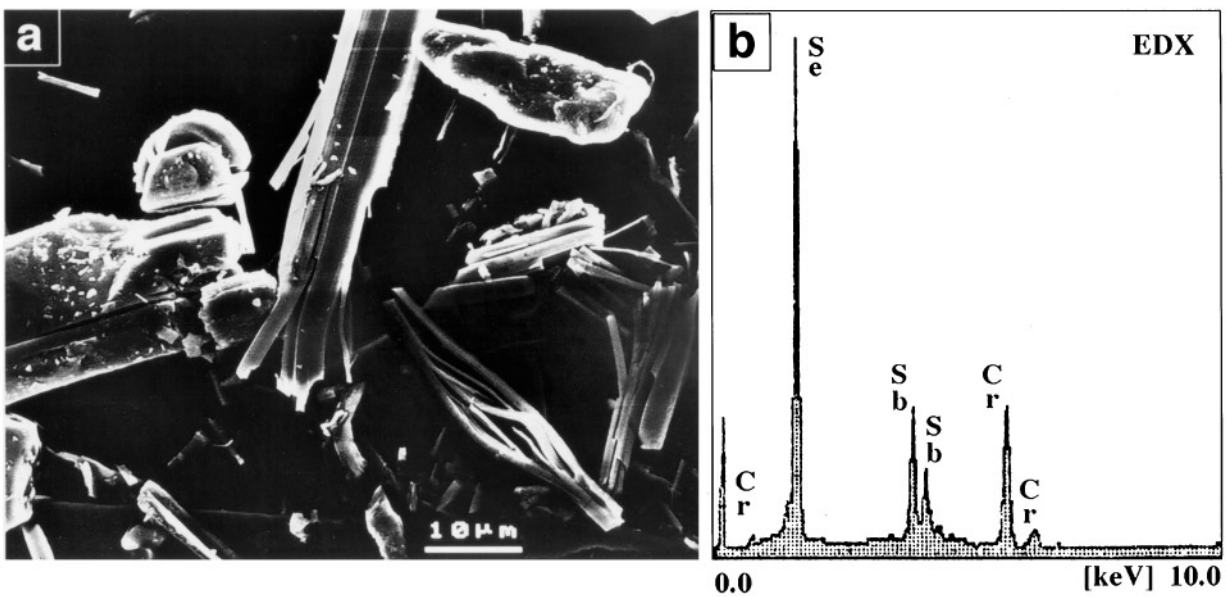

FIG. 1. (a) Scanning electron microscope image of $SbCrSe_3$. Note the deformation and cleavage of the needle-shaped crystals. (b) X-ray microanalysis of the same material.

3. EXPERIMENTAL RESULTS

3.1. SEM and EDX Analysis

According to SEM and EDX data the compounds $SbCrX_3$ ($X = S, Se$) consist predominantly of prismatic needles (Fig. 1a) and have a composition close to that expected (Fig. 1b), although the presence of a small admixture of Sb_2X_3 could not be excluded. Notice that the needles were often curved and split, which suggests a strong anisotropy of the structural and physical properties of the samples analyzed.

3.2. ED and HREM Analysis

3.2.1. HREM structure model. ED patterns show that both compounds are orthorhombic with lattice parameters $a = 9.15$, $b = 3.79$, $c = 13.44$ Å ($SbCrSe_3$) and $a = 8.68$, $b = 3.62$, $c = 12.88$ Å ($SbCrS_3$). The ED patterns of the selenide (insets in Figs. 2 and 3) allow us to derive the following reflection conditions which are compatible with two possible space groups, *Pnma* (No. 62) and $Pna2_1$ (No. 33):

hkl, no conditions; $0kl$, $k + l = 2n$, $h0l$, no conditions;

$hk0$, $h = 2n$; $h00$, $h = 2n$; $0k0$, $k = 2n$; $00l$, $l = 2n$.

The sulfide was assumed to be isostructural to the selenide since it displayed the same reflection conditions.

Direct HREM imaging of the structure and image analysis were applied to determine the $SbCrSe_3$ structure. The HREM image of the structure, viewed along the [100] direction (Fig. 2a), and the symmetry analysis allowed us to eliminate the space group $Pna2_1$ since the $(b \times c)$ cell image displays a center of symmetry (inset in Fig. 2a). A HREM image of the structure viewed along the $[\bar{1}01]$ direction (Fig. 2b), i.e., along the diagonal of the $(a \times c)$ unit mesh, clearly shows the presence of a pair of square-like fragments of size $(b \times b)$ in each unit slice along the *b*-axis; this is shown schematically in the inset of Fig. 3. It suggests that along the *b*-axis the structure may contain double infinite chains of edge sharing $CrSe_6$ octahedra oriented with the apical vortex along $\langle \bar{1}01 \rangle$, since the size of the square-like fragments reflects the typical Se–Se interatomic spacing of $CrSe_6$ octahedra.

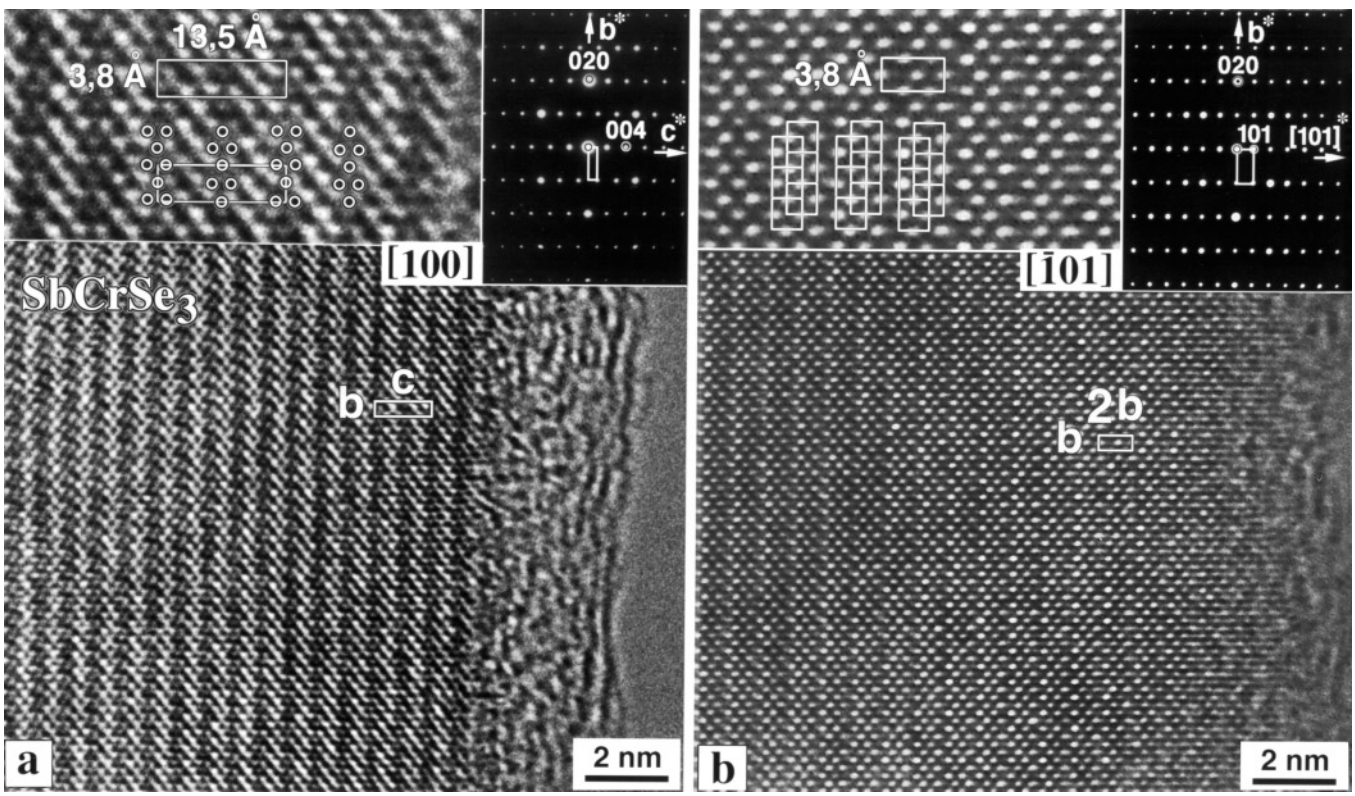

FIG. 2. High-resolution microscope images of the $SbCrSe_3$ structure viewed along [100] zone (a) and $[\bar{1}01]$ zone (b) axis. Near the edge of the specimen the atom columns are imaged as dark dots. The insets show the corresponding diffraction patterns, as well as a higher magnification of the image. The unit mesh is outlined. In the inset of (a) structure elements are highlighted showing the centrosymmetrical character of the image in this projection; in (b) the square-like structure elements are highlighted, suggesting the presence of the double rutile chains formed by pairs of edge sharing octahedra along the [010] direction. The octahedra project as squares of dark dots.

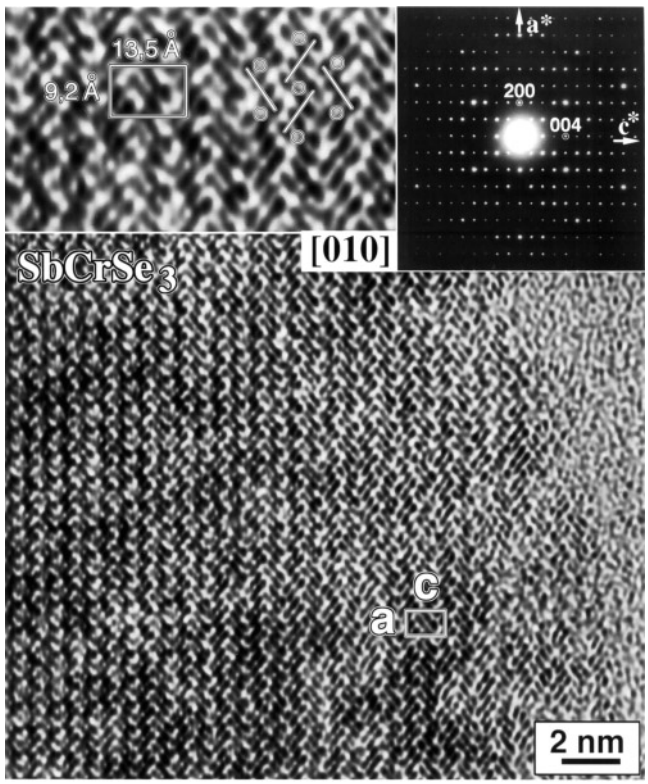

FIG. 3. HREM image of $SbCrSe_3$ along the [010] zone axis. The insets show the corresponding diffraction pattern and a higher magnification of the HREM image. The unit mesh is outlined; the short bars indicate the positions of the double rutile chains. The symmetry elements of this projection are highlighted: the presence of mutually perpendicular traces of glide mirror planes is evident.

This preliminary visual information however is not enough to build a unique structural model. Therefore direct structure imaging and analysis was performed along the [010] direction (Fig. 3), i.e., along the short *b*-axis of the $SbCrSe_3$ structure. The 3.8 Å short *b* parameter, which is along the needle direction, implies that columns along [010] consist of one type of atom; i.e., the structure is a "column structure" along [010]. This is consistent with the HREM images along other directions (Figs. 2a and 2b). The ED pattern along [010] has indeed the largest density of spots (inset, Fig. 3). Under the imaging conditions used (defocus ≈ 40 nm) the atom columns are imaged as dark dots. The image of each $(a \times c)$ unit mesh (Fig. 3) consists of two equivalent fragments (marked by bars in the inset of Fig. 3) related by glide mirror planes. For each fragment the expected composition is $Sb_2Cr_2Se_6$. Image Fourier filtering and image processing were essentially used to improve the experimental image (Fig. 4b), which is part of the HREM image in Fig. 3 taken at a defocus of -40 nm and a crystal thickness of around 3 nm. This information allowed us to propose the structural model shown in Figs. 4c and 4d. Each equivalent fragment consists in turn of two equal parts ($SbCrSe_3$) related by an inversion center (I) in the middle of each bar (inset, Fig. 3); in projection this is represented by a twofold rotation C_2-axis. Only the 4-fold Wyckoff position (4*c*) of *Pnma* satisfies all these symmetry and composition conditions. Therefore for $Z = 4$ only 5×2 independent (x, z) atom coordinates can be determined directly from the image (Fig. 4c). The five remaining *y* atom coordinates can be either 1/4 or 3/4 because of the special Wyckoff position. They have been chosen consistent with the (x, z) atom coordinates from Fig. 4c and with the symmetry elements of the (4*c*) position. Each of the equivalent fragments in turn consists in fact of an infinite double chain of edge sharing $CrSe_6$ octahedra along the *b*-axis (highlighted fragments in Fig. 4d). These chains are separated by Sb atom columns located approximately in pentagonal tunnels of Se atoms. As suggested above, the diagonals of $CrSe_6$ octahedra are indeed oriented along $\langle \bar{1}01 \rangle$ directions in the $(a \times c)$ plane. It is important to note that the 1D chains of $(Sb_2Cr_2Se_6)_n$ form 2D zigzag-like α and β layers along the *a*-axis by the coupling mediated by the shortest Sb–Se bonds as schematically shown in Fig. 4d.

It is clear that the corrugated α and β layers are built from the same structural blocks since they are related by the glide mirror planes. For this reason the compound $SbCrSe_3$ can be classified as a new type of commensurate ABX_3 layered structure. Related structures reported in the literature are those of $MCrSe_3$ with $M =$ Ga (7) and Ce (8), which will be discussed below in relation to our results.

3.2.2. Defect structure. The as-prepared $SbCrSe_3$ compound was relatively free from dislocations and other defects. SEM morphological observations on the layered character of the $SbCrSe_3$ structure have been confirmed by TEM-ED microstructure analysis. In a few cases we observed local cleavage between the α and β layers, resulting in 2D gaps between (001) faces, which indicates that there is indeed a relatively weak chemical bonding between the α and β layers. In some cases it initiated cracks in the material similar to those shown in the SEM micrograph of Fig. 1a. The internal structure within the microcracks was amorphous-like. Dislocations were concentrated predominantly in the local areas near microlamellae of a darker background. Since these darker areas do not generate extra reflections in the diffraction pattern, they are probably due to local inhomogeneity of the material and/or the narrow homogeneity region in the phase diagram around the ideal composition $SbCrSe_3 = 0.5\ Cr_2Se_3 + 0.5\ Sb_2Se_3$. This is in agreement with our attempts to synthesize the material from mixtures of binary selenides such as 0.4/0.6 or 0.6/0.4, which resulted in two-phase mixtures of $SbCrSe_3$ and traces of the majority binary selenide used. Therefore the homogeneity region of $SbCrSe_3$ is expected to be fairly narrow. Apart from dislocations, low angle 2D boundaries or nanocracks

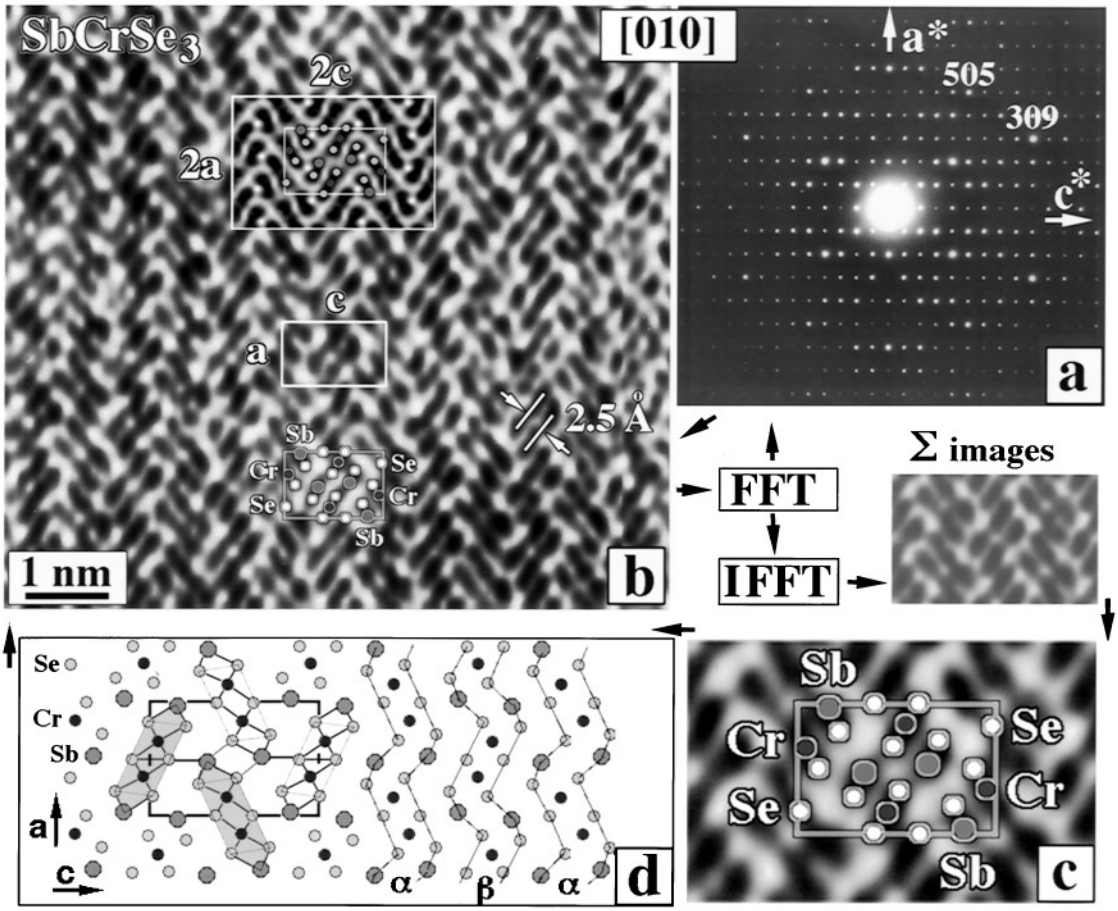

FIG. 4. Successive steps in the processing of the [010] HREM image: (a) Experimental diffraction pattern. (b) Experimental image; atom columns are represented as dark dots at a defocus of -40 nm and a thickness of 3 nm. The larger inset ($2a \times 2c$) is a computer generated image based on the model of (d). This image can be compared with that observed in the smaller frame ($a \times c$). The positions of the atom columns are indicated below. (c) Averaged image obtained by superposition of a ($2a \times 2c$) image fragment with four nearest neighboring similar ones after the Fourier noise filtering (FFT-IFFT). The positions of atom columns are indicated and associated with the black spots in the image. (d) Structure model of $SbCrSe_3$ derived from the image in (c).

parallel to (020) planes with a misorientation between adjacent blocks of $\approx 1^\circ$ were observed by HREM. They are well visible in a cross-sectional view along $[\bar{1}01]$ and may be responsible for the deformed shape of the needle-like crystallites (Fig. 1).

3.3. X-Ray Powder Diffraction: Structure Refinement

The (x, y, z) atom coordinates of the HREM structural model (Figs. 4c and 4d) were directly used as the input for a full profile XRD powder refinement of the $SbCrSe_3$ structure with the help of the program "Rietan-94" (14). It was carried out using the following conditions: space group *Pnma*, fixed y atom coordinates, a block mode for the thermal parameters of Se and Me atoms and under the assumption of [010] preferential orientation. The refined lattice parameters are $a = 9.1689(30)$, $b = 3.7957(12)$, $13.4637(44)$ Å, $D_x = 5.791$ g/cm^3 ($D_m = 5.740$). The residual R factors were $R_F = 2.89$, $R_I = 5.8$, $R_{wp} = 11.29$, $R_p = 8.43\%$. The observed, calculated, and difference X-ray patterns are shown in Fig. 5. The crystallographic parameters, fractional coordinates, and a number of interatomic distances for $SbCrSe_3$ are listed in Tables 1, 2, and 3, respectively. The refined $SbCrSe_3$ structure viewed along [010] is shown in Fig. 6a and Fig. 9b.

All the refined interatomic distances displayed in Table 3 are in agreement with typical Cr–Se, Sb–Se bond lengths and with Se–Se atom spacings in $CrSe_6$ octahedra reported for compounds with a similar composition. As predicted from the HREM model the structure of $SbCrSe_3$ consists of a lattice of infinite double chains of edge sharing $CrSe_6$ octahedra parallel to the b-axis and separated by columns of Sb atoms located approximately in the pentagonal tunnels formed by Se atoms. Sb atoms are shifted in the tunnels in

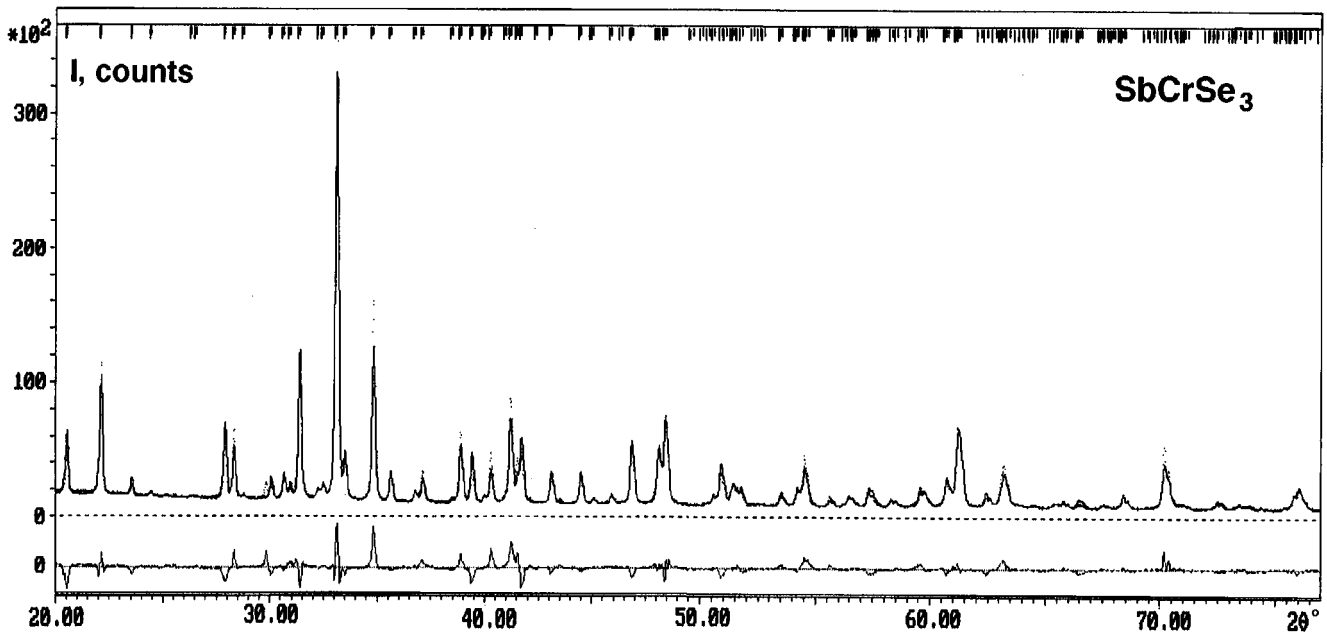

FIG. 5. The observed, calculated, and difference X-ray patterns.

such a way that they form only 3 short chemical bonds with two nearby Se1 atoms and one Se3 atom implying the valence of Sb to be (3 +) and the coordination number to be 6. This fits well with the expected formal charge of Sb as deduced from the stoichiometric formula $Sb^{3+}Cr^{3+}Se_3^{2-}$ since the valence of Cr(3 +) in $CrSe_6$ octahedral coordination is well established. The structure of the $(Sb_2Cr_2Se_6)_n$ atomic chains and of the coordination polyhedra of Cr and Sb are depicted in Figs. 6b and 6c, respectively. As it was predicted from the HREM analysis the Cr polyhedra are almost perfect $CrSe_6$ octahedra (Table 3) whereas the Sb polyhedron can in first approximation be considered a tetragonally distorted $SbSe_6$ octahedron. Strictly speaking, the coordination number of Sb is 6 + 2, because of the bicapped trigonal prism of Se atoms forming a pentagonal tunnel as depicted in Fig. 6c. Notice the absence of direct Se–Se chemical bonds in the structure leading to easy cleavage (001) planes. As one can see, the results of the structural refinement (Fig. 6, Fig. 9b) are in very good agreement with the structure proposed on the basis of the HREM image analysis (Figs. 4c and 4d).

The validity of the refined structural data was verified again by HREM. Figure 7a shows the [120] projection of the structure as deduced from the XRD refinement. A HREM image along this direction shown in Fig. 7b reproduces very well the predicted wavy character of the $SbCrSe_3$ atomic planes represented in Fig. 7a.

3.4. *Magnetic Properties*

As mentioned above, 1D ferromagnetic properties for both compounds ($SbCrX_3$, X = S, Se) can be expected from

TABLE 1
Main Crystallographic Parameters

Empirical formula	$SbCrSe_3$	Cell constants (Å)	
Crystal system	Orthorhombic	a	9.1689(29)
Space group	*Pnma*	b	3.7957(12)
		c	13.4637(44)
Color, habit	Black needles, powder	Volume	468.58(26) Å^3
Z	4	D_x (cal)	5.791
		D_m (g/cm^3)	5.740
Diffractometer	PW3710	$2\theta^\circ$ range	18–80
Radiation, λ(Å)	Cu$K\alpha_{1,2}$	R_I, R_F, R_P, R_{wP}	5.38, 2.89, 8.43, 11.29

TABLE 2
Fractional Coordinates and Thermal Parameters of the Atoms in $SbCrSe_3$

Atom	x/a	y/b	z/c	B_{eq} (Å^2)
Sb	0.46983(30)	0.25	0.65979(23)	0.7(1)
Cr	0.15830(81)	− 0.25	0.54461(56)	0.3(1)
Se1	0.28344(37)	− 0.25	0.71183(36)	0.4(1)
Se2	0.00038(46)	0.25	0.61004(31)	0.4(1)
Se3	0.32896(50)	0.25	0.48437(28)	0.4(1)

magneto-structural considerations. Indeed, the chromium ions Cr(3+) in the octahedral crystal field usually have a high spin $(t_{2g})^3$ orbital state with total spin $S = 3/2$. Since there are no direct metal bonds Cr–Cr and hence t_{2g}–t_{2g} coupling (shortest Cr–Cr interatomic distances are 3.672 and 3.796 Å within the 1D chains and 7.18 and 7.19 Å between them), only superexchange interaction via ligand bridges Cr–Se–Cr between the paramagnetic Cr atoms should be considered in the first approximation. The sign of the interaction is expected to be positive, i.e., a ferromagnetic 90° superexchange in accordance with the empirical rules of Goodenough–Kanamori (15), since all the angles Cr–Se–Cr at the Se atoms in the bridge fragments $SeCr_3$ are very close to 90° (Table 3). Under these conditions the antiferromagnetic (AFM) contribution to the superexchange between the $Cr^{3+}(t_{2g})^3$ orbitals via Cr–Se–Cr bridges reduces to zero and only the ferromagnetic (FM) contribution remains in accordance with the theoretical and experimental analysis of the exchange interactions in Cr dimer clusters (16). In other words, only quasi-1D ferromagnetic superexchange coupling is expected to occur in $SbCrSe_3$. For such particular case the spectrum of magnetic excitations can be expressed well in terms of the spin Hamiltonian for a 1D Heisenberg infinite chain with quantum mechanical spins $S = 3/2$:

TABLE 3
Some Interatomic Distances (Å) and Angles in $SbCrSe_3$

Sb–Se1	2.6482(28) 2×	Se1–Sb–Se1*	91.5°
Sb–Se3	2.6920(55)	Se1–Sb–Se3	85.5°
Cr–Se1	2.5270(99)	Cr–Se2–Cr*	92.5°
Cr–Se2	2.5402(87)	Cr–Se2–Cr	96.4°
Cr–Se2*	2.5445(50) 2×	Cr*–Se2–Cr*	96.4°
Cr–Se3	2.5900(50) 2×	Cr–Se3–Cr	94.3°
Cr–Cr	3.7960(50)	Cr*–Se3–Cr*	94.3°
Cr–Cr*	3.6720(50)		
Se1–Se2	3.4951(47) 2×	Se2–Se3	3.4553(62)

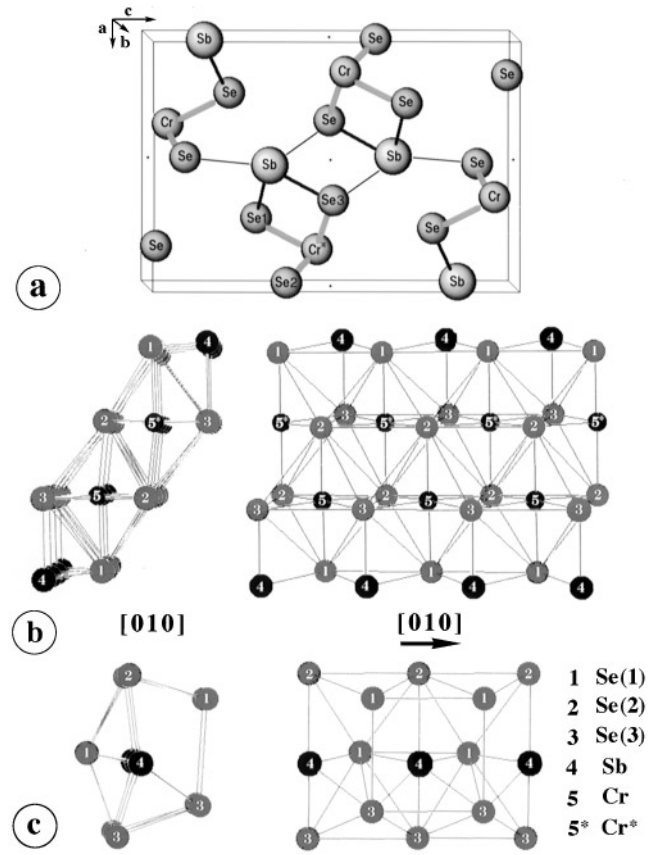

FIG. 6. The $SbCrSe_3$ structure: (a) Perspective view of one unit cell. (b) Perspective construction of the double chain $(Sb_2Cr_2Se_6)_n$ as viewed along the [010] zone axis (left) and perpendicular to this direction (right). (c) Perspective view of the Sb coordination polyhedra forming the pentagonal Se channels viewed along two different directions. The interatomic distances and angles are listed in Table 3.

$$\mathbf{H} = -2\sum_i (J_1 \mathbf{S}_i \mathbf{S}_{i+1} + J_2 \mathbf{S}_i \mathbf{S}_{i+2}) \approx -2J \sum_i (\mathbf{S}_i \mathbf{S}_{i+1} + \mathbf{S}_i \mathbf{S}_{i+2}). \quad [1]$$

Here i denotes the site of a spin on a chain. The exchange parameters may be assumed to be equal $J_1 = J_2 = J$ and positive for the FM case predicted from structural considerations. Such a spin Hamiltonian reflects the magnetic interactions within double Cr chains with $S = 3/2$ schematically shown in Fig. 8a. To our knowledge it has not yet been theoretically analyzed. Strictly speaking, the total magnetic properties of the material can be influenced by the additional weak superexchange coupling between the neighboring FM double Cr chains via the exchange channels of the type Cr–Se–Sb–Se–Cr. Our preliminary attempts to fit the magnetic susceptibility of $SbCrSe_3$ in the framework of a simplified spin Hamiltonian $\mathbf{H} = -2J\sum_i(\mathbf{S}_i\mathbf{S}_{i+1})$ for a 1D

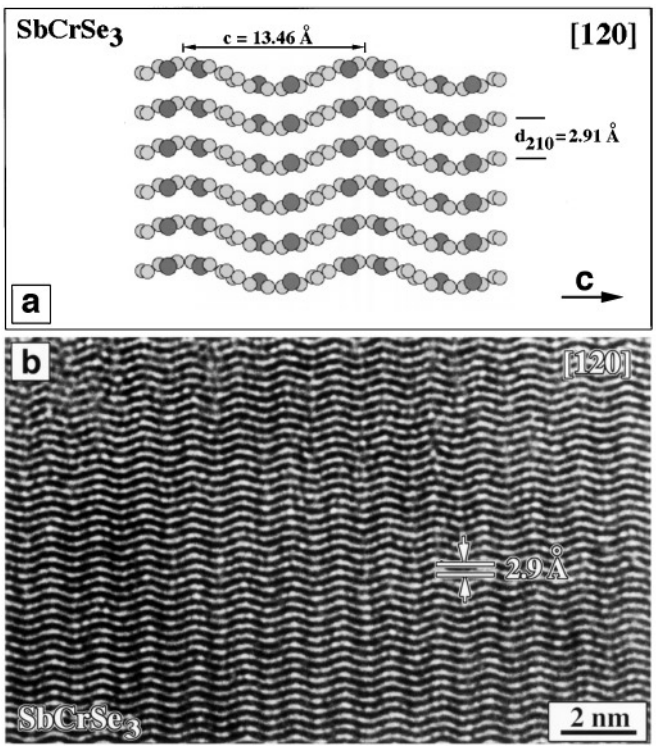

FIG. 7. (a) [120] projection of the structure as predicted by XRD refinement. (b) The corresponding experimental HREM image.

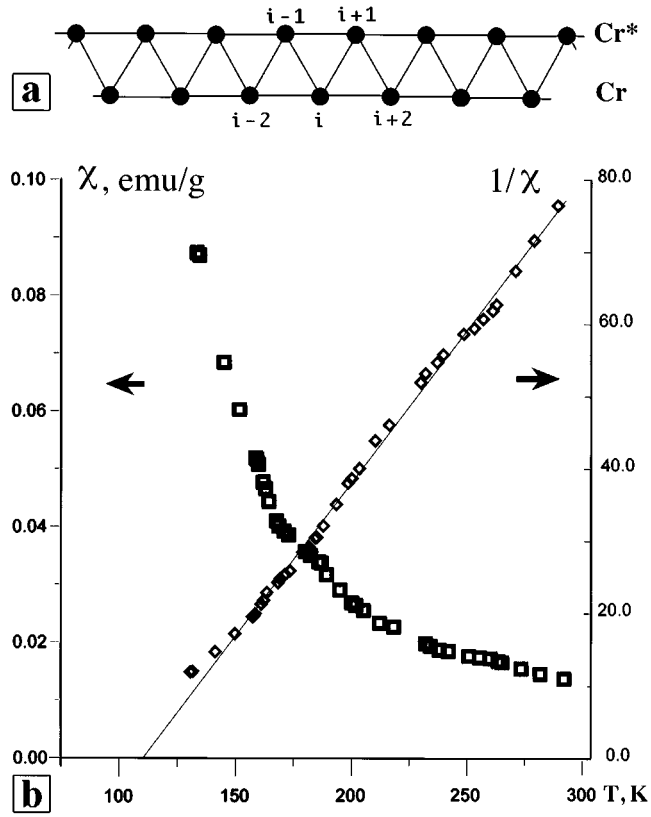

FIG. 8. (a) Schematic configuration of the Cr ions in the double rutile chain along the [010] zone axis, generating the structure of the 1D Heisenberg spin Hamiltonian [1]. (b) Magnetic susceptibility of $SbCrSe_3$ versus temperature. The left ordinate axis refers to χ, whereas the ordinate axis at the right refers to $1/\chi$. Note that the magnetic susceptibility obeys the Curie–Weiss law in the high-temperature range.

Heisenberg infinite chain with $S = 3/2$ required indeed a positive exchange parameter J. A more detailed analysis of the magnetic properties based on the spin Hamiltonian of Heisenberg–Dirac–Van Vleck [1] will be published elsewhere.

In terms of the phenomenological theory of magnetism the observed temperature dependence of the magnetic susceptibility of $SbCrSe_3$ obeys well the Curie–Weiss law in the temperature range 150–300 K,

$$\chi = N\mu_{\text{eff}}^2/3k(T - T_c), \qquad [2]$$

as it is shown in Fig. 8b, with asymptotic Curie temperature $T_c = +110$ K and $\mu_{\text{eff}} = 3.92\,\mu_B$ per one Cr(3+). The μ_{eff} value is very close to the expected value of 3.87 μ_B for Cr(3+) in the paramagnetic state. The effective magnetic moment calculated as $\mu_{\text{eff}} = (8\chi T)^{1/2}$ rapidly increases when approaching T_c. It indicates, in accordance with the analysis made above, that $SbCrSe_3$ undergoes a ferromagnetic transition below the Curie temperature. Similar magnetic behavior was found for the sulfide $SbCrS_3$ ($T_c = +106$ K; $\mu_{\text{eff}} = 3.51\,\mu_B$). Above T_c the compounds display the usual paramagnetic behavior. Below T_c their magnetization depends on the magnetic field H and has a tendency saturate only at low temperatures with a negligible small hysteresis loop (13) indicating the absence of complete FM ordering and hence suggesting the low-dimensional magnetism.

4. DISCUSSION

The structure type of $SbCrSe_3$ (Fig. 9b) is closely related to those of $GaCrSe_3$ (7) and $CeCrSe_3$ (8). As one can see the structure of $SbCrSe_3$ can be considered as intermediate between the cases (a) and (c) in Fig. 9; the rotation angle of the $(M_2Cr_2Se_6)_n$ chains around the b-axis changes when the light element M is replaced by a more heavy one. The M coordination polyhedron undergoes in this way a transformation from a distorted tetrahedron (9a) via a bicapped trigonal prism (9b) toward a tricapped trigonal prism (9c) resulting in coordination numbers $CN = 4$, $CN = 6 + 2 = 8$, and $CN = 9$, respectively. The structure type of $SbCrSe_3$ may be useful for structure determination of at least some of the complex chalcolantanides with the general formulas $LnCrX_3$, Ln_3CrX_6, $LnCr_3X_6$ (Ln = rare

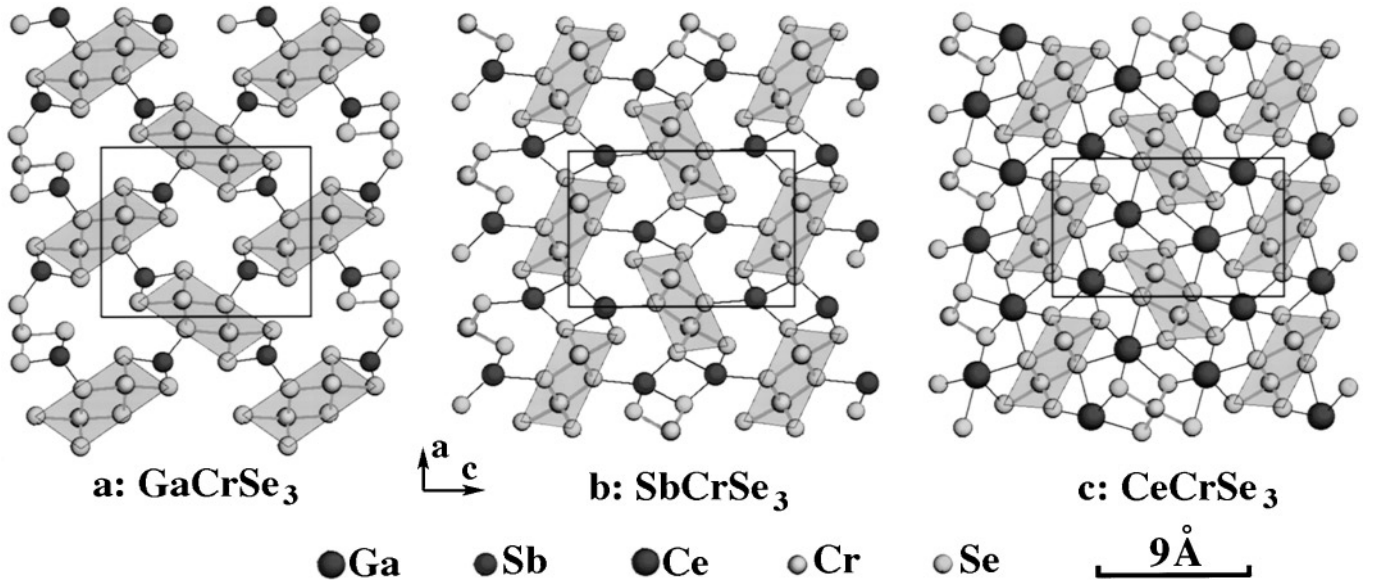

FIG. 9. Comparison of the structure models of three related structure types viewed along homologous zone axes: (a) $GaCrSe_3$ (7), (b) $SbCrSe_3$ (present work), and (c) $CeCrSe_3$ (8). The double chains of Cr sharing octahedra are highlighted. In structures of the type (a) and (b) a 1D ferromagnetism is expected to occur.

earth, $X = S, Se$) reviewed in (17). For many of these the crystal structures (of orthorhombic and/or monoclinic symmetry) are not determined yet. Among the determined structures only sulfides with monoclinic cells (Ln = La, Gd, Y, Ho, Er), orthorhombic $DyCr_3S_6$, and selenides with orthorhombic cells (Ln = La, Ce, Pr, Nd) are present. The last crystallize in the $CeCrSe_3$ structure type (Fig. 9c). It was shown that most of these chalcolantanides are semiconducting antiferromagnets except for $GdCrX_3$ (X = S, Se, Te), which were found to be ferromagnets. In contrast to $GdCrX_3$, two new orthorhombic structures of $GdCr_3S_6$ (or $Gd_{2/3}Cr_2S_4$) (18) and Gd_3CrSe_6 (19) have been determined, which display "simple" paramagnetic behavior down to liquid helium temperature, although for $GdCr_3S_6$ a magnetic anomaly at 70–100 K was noticed.

We believe that the exceptional ferromagnetism of $GdCrTe_3$ (T_c = 220 K) and $GdCrS_3$ (T_c = 110 K) from the family of semiconducting antiferromagnetic chalcolantanides can be understood in terms of our results for $SbCrX_3$ (X = S, Se) for two reasons. First, Gd(3+), unlike other Ln, is characterized by the absence of spin–orbital interaction because of its term $^8S_{7/2}$. This means that its magnetic moment is formed only by 4f electrons and its magnetic properties will be governed similar to the case of Cr(3+) only by spin exchange interactions. Second, from the above considerations they seem to be isostructural with one of the types depicted in Figs. 9b and 9c. In our opinion the structure type of $SbCrSe_3$ (Fig. 9b) is the more preferable one, since $CN = 6 + 2 = 8$ of Sb ions better agrees with the expected CN for Gd ions in related structures. Indeed, similar bicapped trigonal prisms of X atoms, like those centered by Sb in $SbCrSe_3$ (Fig. 6c, left inset), were found to be centered by Gd ions in $GdCr_3S_6$ (18) and Gd_3CrSe_6 (19).

Finally, the hypothetical replacement of nonmagnetic Sb(3+) by magnetic Gd(3+) can give rise to the formation of 1D ferromagnetism in $GdCrS_3$ (highly distorted "$SbSe_6$" octahedron; $CN = 6 + 2$) similar to that observed for $SbCrX_3$ (T_c = 100–110 K). Alternatively it may, perhaps, result in 2D ferromagnetism of $GdCrTe_3$ (nondistorted "$SbSe_6$" octahedron, analogue of "$CrSe_6$," $CN \approx 6$), where double chains of CrT_6 octahedra will be bonded via $GdTe_6$ octahedra into 2D α- and β-ferromagnetic layers. In view of this prediction the higher T_c for $GdCrTe_3$ compared to $SbCrX_3$ would simply reflect the change in dimension from 1D to 2D magnetism according to the model of the exchange channels (20). Notice that along with the similarity of the structural blocks of $GdCr_3S_6$ and Gd_3CrSe_6 to our case of $SbCrSe_3$ the former do not display any ferromagnetism in contrast to what was found in $GdCrS_3$ (T_c = 110 K) and $GdCrTe_3$ (T_c = 220 K (17), since only the structure types shown in Figs. 9a and 9b can give rise to 1D or 2D ferromagnetism in accordance with our magneto-structural considerations mentioned above.

5. CONCLUSIONS

The combined use of HREM imaging, image analysis, and powder X-ray refinement techniques enabled us to obtain accurate structural data for powdered $SbCrSe_3$. We believe that the new structure type and the unusual magnetic properties of $SbCrX_3$ may be useful for the characterization by analogy of at least some of the complex chalcolantanides with the general formulas $LnCrSe_3$, Ln_3CrSe_6, and $LnCr_3Se_6$. Many of these the crystal structures and superstructures are not determined yet, but we note that the ratios of the lattice parameters are close to those of $SbCrX_3$, suggesting a strong similarity of the structures.

After having completed the redaction of our manuscript we discovered an independent structure determination of the same materials $SbCrS_3$ (21) and $SbCrSe_3$ (22) based on single crystal X-ray data and with reference to our earlier work (13) on synthesis and magnetism of $SbCrS_3$. The conclusions concerning the crystal structure and magnetic properties of the materials are the same, although the structural methods used were different. In our study only powdered materials were available. Therefore our paper illustrates how the combined extensive use of HREM, electron microdiffraction, and powder X-ray diffraction allows one nevertheless to determine a relatively complicated structure to an accuracy comparable to that obtained by a single crystal X-ray diffraction.

ACKNOWLEDGMENT

V. V. Volkov is grateful to the Belgian Science Policy Office for his DWTC fellowship in 1996.

REFERENCES

1. F. K. Lotgering and G. H. A. M. van der Steen, *J. Inorg. Nucl. Chem.* **33,** 673 (1971).
2. Dismukes *et al.*, *Z. Kristallogr.* **132,** 272 (1971).
3. H. Noel *et al.*, *C.R. Seances Acad Sci., Ser. C* **280,** 123 (1975).
4. Takahashi *et al.*, *Mater. Res. Bull.* **6,** 173 (1971).
5. R. Brec *et al.*, *Ann. Chim.* (*Paris*) **5,** 499 (1980).
6. H. Noel, *Rev. Chim. Miner.* **14,** 295 (1977).
7. H. Lutz *et al.*, *Z. Anorg. Allg. Chem.* **566,** 55 (1988).
8. Huy-Dung *et al.*, *Bull. Soc. Chim. Fr.* 2433 (1971).
9. O. Gorochov and H. McKinzie, *J. Solid State Chem.* **7,** 400 (1979).
10. K. Kato, *Acta Crystallogr. B* **46,** 39 (1990).
11. T. B. Williams and B. G. Hyde, *Acta Crystallogr. B* **4,** 467 (1988).
12. S. M. Maruk, R. A. Sadykov, T. G. Aminov, E. V. Amerikova, and A. V. Rudnev, "Proceedings IOFAN, Vol. 44, Fotomagnetism, p. 173. Nauka, Moscow, 1993.
13. K. P. Belov, L. T. Koroleva, N. P. Pislyakova, E. E. Amerikova (Busheva), G. G. Shabunina, and T. G. Aminov, *Inorg. Mater.* **27,** 1873 (1991); *Inorg. Mater.* (*Russ.*) **27,** 2199 (1991).
14. F. Izumi, *in* "The Rietveld Method" (R. A. Young, Ed.), Chap. 13. Oxford Univ. Press, Oxford, 1993.
15. J. B. Goodenough, "Magnetism and the Chemical Bond." Wiley, New York, 1986.
16. Yu. V. Rakitin, and V. V. Volkov, *Khoord. Khim.* (*Rus*) **12,** 1509 (1986).
17. P. G. Rustamov, O. M. Aliev, and T. X. Kyrbatov, "Chalcolantanides of the Rare Earth Elements," p. 284. Science (Russ.), Moscow, 1989.
18. A. Meerschaut, A. Lafond, L. M. Hoistad, and J. Rouxel, *J. Solid State Chem.* **111,** 276 (1994).
19. G. G. Guseinov, V. A. Gasumov, I. P. Aliev, and Kh. S. Mamedov, *Inorg. Mater.* (*Russ.*) **17,** 556 (1981).
20. M. V. Eremin and Yu. V. Rakitin, *Phys. Stat. Sol.* (*b*) **80,** 579 (1977); *Phys. Stat. Sol.* (*b*), **82,** 221 (1977) *Phys. Stat. Sol.* (*b*) **85,** 783 (1978).
21. S. Jobic, P. Le Boterf, F. Bodénan, and G. Ouvrard, *C.R. Acad. Sci. Paris* **318,** 893 (1994).
22. D. A. Odink, V. Carteaux, C. Payen, and G. Ouvrard, *Chem. Mater.* **5,** 237 (1993).